Body centered cubic carbon BC14: An all-sp^3 bonded full-fledged pentadiamond

Jian-Tao Wang [1,2,3,*] Changfeng Chen,[4] and Hiroshi Mizuseki [5]

[1]*Beijing National Laboratory for Condensed Matter Physics, Institute of Physics, Chinese Academy of Sciences, Beijing 100190, China*
[2]*School of Physical Sciences, University of Chinese Academy of Sciences, Beijing 100049, China*
[3]*Songshan Lake Materials Laboratory, Dongguan, Guangdong 523808, China*
[4]*Department of Physics and Astronomy, University of Nevada, Las Vegas, Nevada 89154, USA*
[5]*Computational Science Research Center, Korea Institute of Science and Technology, Hwarangno 14-gil 5,
Seongbuk-gu, Seoul 02792, Republic of Korea*

We report on the finding of a hard carbon structure in body centered cubic ($I2_13$) symmetry that possesses an extremely high bulk modulus (386 GPa) and Vickers hardness (60 GPa) comparable to that of *c*-BN and diamond. This carbon phase has a 14-atom primitive cell in an all-sp^3 bonding network comprising five-membered rings, making it a truly full-fledged pentadiamond. Total energy calculations show that it is more stable than the previously reported diamondlike six-membered-ring bonded BC8 and BC12 carbon phases. Electronic band structure calculations show that it is an insulator with an indirect band gap of 5.64 eV. Simulated x-ray diffraction patterns and lattice parameters provide an excellent match to the previously unexplained distinct diffraction peaks found in carbon soot. The present results establish a distinct type of carbon phase and offer insights into its outstanding structural, mechanical, and electronic properties.

I. INTRODUCTION

Carbon exhibits extremely versatile bonding abilities that produce a rich variety of crystalline forms with novel properties in sp^3-, sp^2-, and sp-hybridized bonding states [1–7]. At ambient conditions, graphite is the thermodynamically most stable carbon allotrope with strong in-plane aromatic π conjugation. A rich variety of carbon phases has also been synthesized under laboratory conditions [4–6,8–22], such as fullerenes [8], carbon nanotubes [9], graphene [10], and graphdiyne [11]. A useful way is to explore new carbon allotropes under extreme conditions such as high pressure or shock compression. Cold-compressed graphite [23] at room temperature has led to the identification of several new hard carbon structures [24–35] such as monoclinic *M*-carbon [24], orthorhombic *W*-carbon [26], and *Z*-carbon [28]. In addition, a new cubic modification of carbon denoted BC12 in $Ia\bar{3}d$ symmetry [36] was proposed to be a likely candidate structure found in shock-compressed tetracyanoethylene powder [37] and bcc carbon BC8 [38] was reported to be the high-pressure modification of carbon derived from cubic diamond under a pressure of ∼1100 GPa [38–41] and was identified in diamondlike carbon thin films [42]. Meanwhile, the supercubane (cub-C_8) was theoretically predicted [43] and synthesized from amorphous carbon films by using a pulsed-laser-induced liquid-solid interface reaction [44]. Recently, *T*-carbon [12] was produced from pseudotopotactic conversion of a multiwalled carbon nanotube suspension in methanol by picosecond pulsed-laser irradiation [45], despite

its rather high energy of about 1.2 eV per atom above that of diamond and graphite [46]. The design and synthesis of new carbon structures are one of the hot issues in condensed-matter physics because of their fascinating properties. Very recently, the so-called two-dimensional pentagraphene [47] and three-dimensional pentadiamond (FC22) [48] were also suggested with sp^2- and sp^3-hybridized pentagonal networks.

In this paper, by combining a systematic structure search process and *ab initio* calculations, we identify a hard carbon structure comprising five-membered rings in an all-sp^3 bonding network, characterized as a truly full-fledged pentadiamond. This new carbon polymorph has a 14-atom primitive cell in bcc ($I2_13$) symmetry and is thus termed BC14 carbon. Its dynamic structural stability has been verified by phonon mode analysis. Total energy calculations show that it is energetically more stable than the previously reported BC8 [39], BC12 [36], and cub-C_8 [43] carbon phases. Electronic band structure calculations show that it is an insulator with an indirect band gap of 5.64 eV, thus expected to be optically transparent. Remarkably, BC14 carbon possess an extremely high bulk modulus (386 GPa) and Vickers hardness (60 GPa), which are comparable to the corresponding values of *c*-BN and diamond. Moreover, a good match between the simulated and measured x-ray diffraction patterns makes a strong case for assigning BC14 carbon as the experimentally observed new carbon phase in carbon soot [49].

II. COMPUTATIONAL METHODS

We have performed a structure search using a technique based on a Monte Carlo algorithm [50]. The energetics were first screened by highly efficient Tersoff potential calculations

*wjt@aphy.iphy.ac.cn
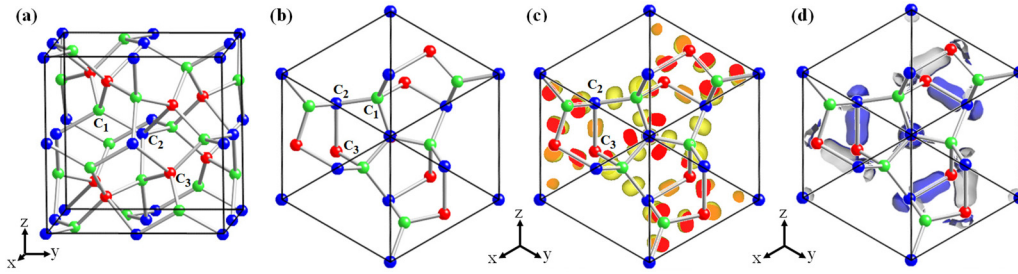
FIG. 1. Crystalline structure of BC14 carbon in $I2_13$ (T^5, No. 199) symmetry. (a) A 28-atom cubic unit cell with a lattice parameter of a = 5.5453 Å, occupying $12b$ (0.3701, 0.0, 0.25), $8a$ (0.9931, 0.9931, 0.9931), and $8a$ (0.1830, 0.1830, 0.1830) Wyckoff positions, denoted by C_1, C_2, and C_3, respectively. (b) A 14-atom primitive cell with lattice parameters of a = 4.8024 Å and α = 109.47°. The carbon atoms form five-membered rings in an all-sp^3 bonding network, characterized as pentadiamond. (c) Electron localization function (ELF) map for BC14 carbon with an isosurface level of 0.82. (d) Partial charge density distribution of the topmost valence band with an isosurface level of 0.06 $e/\text{Å}^3$, mainly coming from the C_2 and C_3 atoms.

[51] and then refined by more accurate first-principles methods. This targeted search resulted in the identification of BC14 carbon in a 28-atom cubic cell. Density functional theory calculations are performed using the Vienna Ab initio Simulation Package (VASP) [52]. The generalized gradient approximation developed by Armiento and Mattsson (AM05) [53] is adopted for the exchange-correlation potential. The all-electron projector augmented wave [54] method is adopted, with $2s^2 2p^2$ treated as valence electrons. Wave functions of the valence electrons are expanded in plane waves up to a kinetic energy cutoff of 800 eV, and the Brillouin zone is sampled with a $10 \times 10 \times 10$ Monkhorst-Pack special k-point grid including the Γ point. Convergence criteria employed for both the electronic self-consistent relaxation and the ionic relaxation are set to 10^{-8} eV and 0.01 eV/Å for energy and force, respectively. Electronic band structures are calculated using the Heyd-Scuseria-Ernzerhof hybrid functional (HSE06) [55]. Phonon calculations are performed using the PHONOPY package [56].

III. RESULTS AND DISCUSSION

We first present the structural characterization of BC14 carbon. It has a 28-atom bcc unit cell in $I2_13$ (T^5) symmetry [see Fig. 1(a)] with three irreducible atom sites occupying the $12b$ (0.3701, 0.0, 0.25), $8a$ (0.9931, 0.9931, 0.9931), and $8a$ (0.1830, 0.1830, 0.1830) Wyckoff positions, denoted by C_1, C_2, and C_3, respectively. There are three distinct bond lengths of 1.547 Å (C_1-C_2), 1.498 Å (C_1-C_3), and 1.824 Å (C_2-C_3). Also, there are five different bond angles, 92.33° for $\angle C_3$-C_1-C_3, 98.75° for $\angle C_1$-C_3-C_2, 115.89° for $\angle C_1$-C_2-C_1, 117.33° for $\angle C_1$-C_3-C_1, and 121.26° for $\angle C_2$-C_1-C_2. These bond angles are averaged and equal to 109.11°, close to 109.47° in diamond with a large bond angle range from 92.33° to 121.26°, similar to the findings in all-sp^3 BC12 [36] and R16 carbon [50]. A 14-atom primitive cell is also given in Fig. 1(b). The carbon atoms form five-membered carbon rings in an all-sp^3 bonding network, characterized as pentadiamond. Remarkably, the lattice parameters are estimated to be a = 5.545 Å, which is in good agreement with the experimental lattice data for an unidentified cubic carbon phase [35].

To understand the bonding nature of electrons in BC14 carbon, the electron localization function (ELF) map is illustrated

in Fig. 1(c) with an isosurface of 0.82. The high ELF values (1> ELF > 0.5) indicate the formation of covalent bonds [57]. We can see that the electrons are well localized in between the C_2-C_3 bonds as well as in between the C_1-C_2 and C_1-C_3 bonds [58], showing the typical covalent bonding behavior between carbon atoms in BC14 pentadiamond.

Figure 2 presents the total energy as a function of volume per atom for BC14 carbon, in comparison with graphite, diamond, BC8 [39], BC12 [36], cub-C_8 [46], Rh6 polybenzene [15], and FC22 pentadiamond [48]. Among these carbon allotropes, BC8 and BC12 as well as diamond comprise six-membered carbon rings. It can be seen that BC14 is obviously less stable than graphite, diamond, Rh6 polybenzene, and FC22 pentadiamond but energetically more stable than BC8, BC12, and the cub-C_8 carbon phase, with a substantial energy gain of 0.177, 0.383, and 0.162 eV per carbon atom, respectively, suggesting better thermodynamic stability of BC14 carbon. Meanwhile, BC14 has a smaller volume than cub-C_8, Rh6 polybenzene, and FC22 pentadiamond, showing a denser
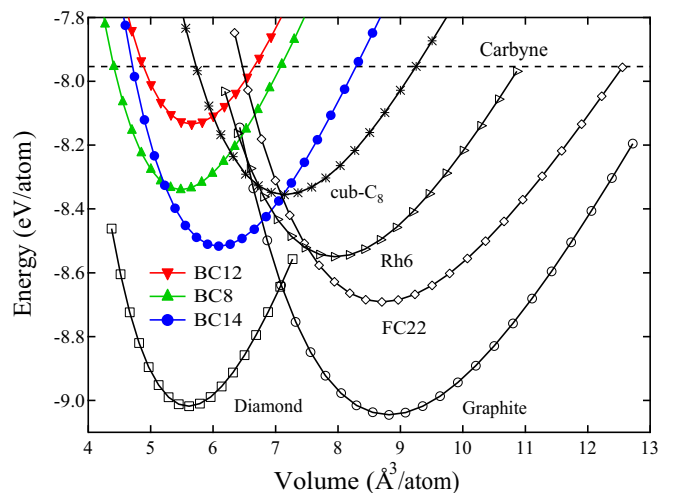
FIG. 2. The total energy as a function of volume per atom for the BC14 carbon phase in comparison with graphite, diamond, cub-C_8 [44], BC8 [39], BC12 [36], Rh6 polybenzene [15], and FC22 pentadiamond [48]. The dashed line indicates the energy level of the linear carbyne chain.

TABLE I. Calculated equilibrium structural parameters (lattice parameters a and c, volume per atom V_0, density ρ, and bond lengths d_{C-C}), total energy per atom E_{tot}, electronic band gap E_g, bulk modulus B_0, and Vickers hardness H_v for graphite, diamond, cub-C_8, BC8, BC12, BC14, Rh6, and pentadiamond (FC22), compared to available experimental data (EXP) [35,37,42,62,63].

Structure	Space group	Method	a (Å)	c (Å)	V_0 (Å^3)	ρ (g/cm^3)	d_{C-C} (Å)	E_{tot} (eV)	E_g (eV)	B_0 (GPa)	H_v (GPa)
Diamond	$Fd\bar{3}m$	AM05	3.552		5.60	3.56	1.538	−9.018	5.36	451	93.5
		EXP [62]	3.567		5.67	3.52	1.544		5.47	446	96 [63]
Cub-C_8	$Im\bar{3}m$	AM05 [46]	4.853		7.15	2.79	1.470, 1.578	−8.355	4.17	323	31.0
BC8	$Ia\bar{3}$ [39]	AM05	4.443		5.48	3.64	1.455, 1.617	−8.340	3.58	412	82.5
		EXP [42]	4.450								
BC12	$Ia\bar{3}d$ [36]	AM05	5.139		5.66	3.53	1.574	−8.134	2.98	429	76.7
		EXP [37]	5.140								
BC14	$I2_13$	AM05	5.545		6.09	3.27	1.498−1.824	−8.517	5.64	386	59.5
		EXP [35]	5.545								
Rh6	$R\bar{3}m$	AM05 [15]	6.902	3.470	7.96	2.50	1.359, 1.483	−8.550	0.47	291	9.7
FC22	$Fm\bar{3}m$ [48]	AM05	9.148		8.71	2.29	1.348−1.556	−8.691	3.52	258	22.3
Graphite	$P6_3/mmc$	AM05	2.462	6.710	8.81	2.26	1.422	−9.045		280	
		EXP [62]	2.460	6.704		8.78	1.420			286	

carbon phase with a larger density of 3.27 g/cm^3. In order to obtain the bulk modulus B_0, we fit the energy-volume data to the higher-order Birch-Murnaghan equation of state $E(V) = \sum [a(n)V^{-2n/3}]_{n=0,m}$, with $m = 5$ or 6, and the fitting coefficient $a(n)$ is obtained using a least-squares fit [59,60]. The bulk modulus B_0 for BC14 carbon is estimated to be 386 GPa [401 GPa under the local density approximation (LDA)], which is about 14% smaller than the value of 451 GPa for diamond (466 GPa under LDA) but almost equal to the value of 386 GPa for c-BN (396 GPa under LDA [61]), suggesting the potential for BC14 carbon in a superhard material. The calculated equilibrium structural parameters, total energy, and bulk modulus are listed in Table I and are compared to available experimental data [35,37,42,62].

To confirm the mechanical stability, we have calculated the elastic constants C_{ij} for BC14 carbon as $C_{11} = 836$ GPa, $C_{12} = 162$ GPa, and $C_{44} = 404$ GPa. These results satisfy the mechanical stability criteria $C_{11} > 0$, $C_{44} > 0$, $C_{11} > |C_{12}|$, and $C_{11} + 2C_{12} > 0$ for the cubic structure [64].

We have also estimated both bulk modulus B and shear modulus G values from the elastic constants [64] in comparison with c-BN and diamond. The bulk modulus B is estimated to be 387 GPa for BC14, 388 GPa for c-BN, and 454 GPa for diamond, which are well in agreement with the data (see Table I for BC14 and diamond) obtained by the Birch-Murnaghan fit of the energy-volume curves; meanwhile, the shear modulus G is estimated to be 377 GPa for BC14, 400 GPa for c-BN, and 537 GPa for diamond. Based on these B and G data, we then calculate the Vickers hardness H_v using the empirical formula $H = 2(G^3/B^2)^{0.585} - 3$, suggested by Chen et al. [63]. The H_v values are estimated to be 59.5 GPa for BC14, 66.0 GPa for c-BN, and 93.5 GPa for diamond. Our calculated B, G, and H_v values for c-BN and diamond are well in agreement with the previously reported data [63]. Meanwhile, the values for BC14 carbon are smaller than that of diamond but very close to the data for c-BN. These results suggest BC14 is a hard material, like c-BN and diamond.

For comparison, we have also calculated the elastic constants C_{ij} for the recently reported FC22 pentadiamond [48] as $C_{11} = 552$ GPa, $C_{12} = 114$ GPa, and $C_{44} = 142$ GPa. B, G, and H_v are estimated to be $B = 260$ GPa, $G = 173$ GPa, and $H_v = 22.3$ GPa, which are well in agreement with the data given by Brazhkin et al. [65] and Saha et al. [66]. We can see that the proposed FC22 pentadiamond is, indeed, not able to be a hard material since it is not dense [67,68], with a small density of 2.29 g/cm^3 (see Table I).

To confirm the dynamical stability, we have calculated the phonon band structures and partial density of states (PDOS). As shown in Fig. 3, the highest phonon frequency of 1348 cm^{-1} is at the Γ point, relative to the C_1 and C_3 atoms with a bond length of 1.498 Å (C_1-C_3). Meanwhile, there is a gap between 1201 and 1280 cm^{-1}, and PDOS peaks around 1195 cm^{-1} are mainly relative to the C_1 and C_2 atoms with a bond length of 1.547 Å (C_1-C_2). The highest phonon frequency of 1348 cm^{-1} in BC14 is close to ∼1326 cm^{-1} in diamond [69]. Moreover, throughout the entire Brillouin
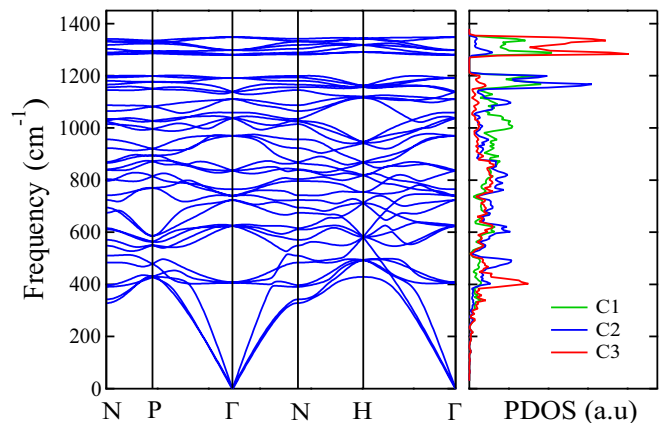
FIG. 3. Phonon band structures and PDOS for BC14 carbon at equilibrium lattice parameters. The highest phonon frequency of 1348 cm^{-1} is at the Γ point.
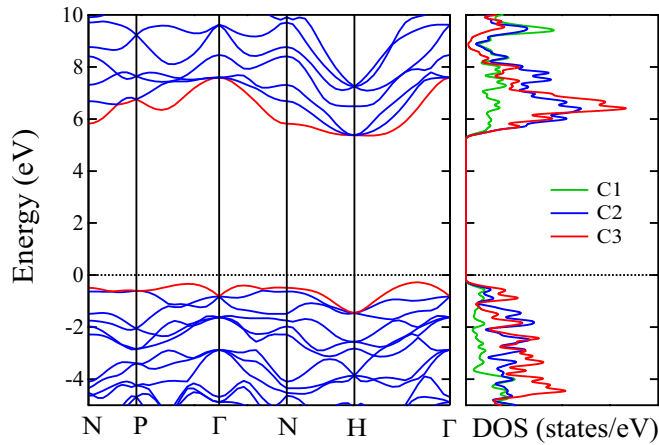
FIG. 4. Electronic band structures and DOS for BC14 carbon. The calculations are performed using the HSE06 method at equilibrium lattice parameters.

zone, no imaginary frequencies are observed, confirming the dynamic stability of BC14 carbon.

The electronic band structures and density of states (DOS) are calculated based on the hybrid density functional method (HSE06) [55]. As shown in Fig. 4, the conduction band minimum (CBM) and valence band maximum (VBM) are located along the Γ-H direction, showing an insulator behavior with an indirect band gap of 5.64 eV. This band gap is close to the data for W-carbon (5.69 eV) [32,33] and even appreciably larger than the gap (5.47 eV) for diamond. Therefore, BC14 carbon is expected to be optically transparent. Meanwhile, from the projected density of states and band-decomposed partial charge density distribution [see Fig. 1(d)], we can see that the states near the CBM and VBM points mainly come from the C_2 and C_3 atoms.

As mentioned above, the calculated lattice parameters for BC14 are in good agreement with the experimental lattice data for an unidentified cubic carbon phase [35]. To further establish the experimental connection of BC14 carbon, we simulated the x-ray diffraction (XRD) spectra of BC14 carbon as well as those for graphite, diamond, BC8, Rh6 polybenzene, cub-C_8, and FC22 pentadiamond [see Fig. 5(a)] and compared the results with experimental XRD data of carbon soot [49]. As shown in Fig. 5(b), the measured XRD spectra reveal a considerable amount of amorphous carbon and provide clear evidence for several crystalline phases in the recovered specimen. The most distinct feature is a sharp peak at 30°, which has been attributed to the Rh6 (101) diffraction [15,70], and the small peak around 43.7°, matching that of diamond (111) diffraction, indicates the presence of a small amount of diamond. Meanwhile, a strong peak at 23° and a small peak at 40° do not match any previously known carbon phases such as BC8, cub-C_8, and FC22 pentadiamond. Our simulated XRD results for BC14 carbon show that the main BC14 (110) diffraction peak perfectly matches the unexplained measured peak at 23°, and the small peak of BC14 (211) matches well the peak at 40° in measured XRD spectra. These results suggest that BC14 carbon is a likely candidate for the carbon phase observed in the chimney carbon soot [49].
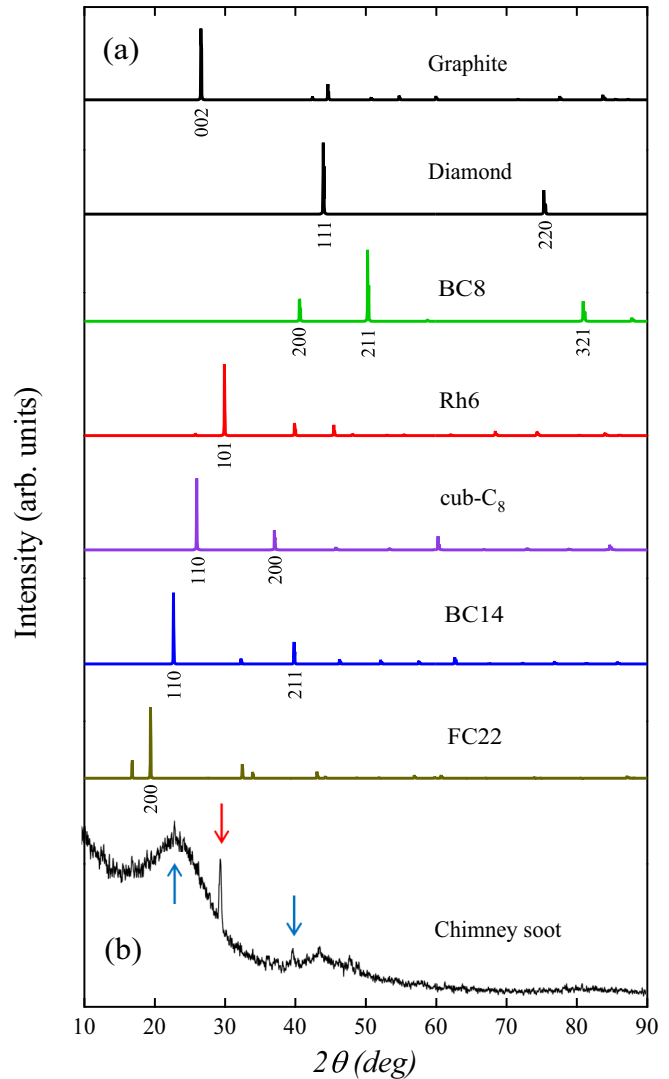
FIG. 5. (a) Simulated XRD patterns for graphite, diamond, BC8, Rh6, cub-C_8, BC14 carbon, and FC22 pentadiamond. (b) Experimental XRD patterns for the chimney soot [49]. The x-ray wavelength is 1.5406 Å with a copper source.

Besides this insulating BC14 pentadiamond phase in $I2_13$ (No. 199) symmetry, we have also predicted a metallic BC14 carbon structure in $I\bar{4}3d$ (No. 220) symmetry. The lattice parameters are estimated to be $a = 5.570$ Å, occupying two Wyckoff positions, 12b (0.8750, 0.0, 0.25) for C_1 and 16c (0.2152, 0.2152, 0.2152) for C_2. The bond lengths between C_1 and C_2 atoms are 1.507 Å. Each C_1 atom has four C_1-C_2 bonds with bond angles of 107.51°–110.46° for $\angle C_2$-C_1-C_2; meanwhile, each C_2 atom has three C_1-C_2 bonds with a bond angle of 119.81° for $\angle C_1$-C_2-C_1, showing an $sp^2 + sp^3$-hybridized network. However, it is energetically less stable than the BC14 pentadiamond phase with an energy loss of 0.212 eV per atom and dynamically unstable for larger imaginary frequencies. As a result, the unfavorable sp^2-type 16c C_2 atoms divide into two sp^3-type C_2 and C_3 atoms to form the BC14 pentadiamond.

There are currently more than 500 carbon structures in all-sp^2, all-sp^3, $sp + sp^2$, $sp + sp^3$, and ($sp^2 + sp^3$)-hybridized

bonds registered to the Samara Carbon Allotrope Database [71]. Also, 43 new superhard carbon phases were predicted in a recent study [72]. Among these carbon allotropes, only BC8 [38–41], BC12 [36], and R16 carbon [50] are composed of six-membered carbon rings in addition to diamond, but they are energetically less stable than diamond due to the larger bond distortions [36,50]. For example, there are two different bond angles of 99.59° and 131.81° with a bond length of 1.574 Å in all-sp^3 BC12 carbon [36]; meanwhile, R16 carbon contains four distinct bond lengths of 1.457, 1.488, 1.569, and 1.748 Å with a varying bond angle ranging from 100.13° to 120.68° [50]. The stability for these synthesized metastable carbon structures can be understood by their kinetic barrier. A larger kinetic barrier can slow down or prevent the phase transition at room temperature, such as those found in the diamondlike carbon [26,31,73], BC8 silicon, and ST12 germanium [74].

IV. SUMMARY

In summary, by combining a systematic structure search process and *ab initio* calculations, we have identified a hard carbon structure in bcc ($I2_13$) symmetry with an all-sp^3 five-membered-ring bonding network. This truly full-fledged pentadiamond phase is energetically more stable than previ-ously reported BC8, BC12, and cub-C_8 carbon phases and is dynamically stable. Electronic band structure calculations showed that it is an insulator with an indirect band gap of 5.64 eV, expected to be optically transparent like diamond. Remarkably, this carbon phase possesses an extremely high bulk modulus (386 GPa) and Vickers hardness (60 GPa) in comparison to those of *c*-BN, presenting as a hard carbon ma-terial. Moreover, the good match between the simulated and measured x-ray diffraction patterns suggests that BC14 carbon with five-membered rings as well as Rh6 polybenzene may be present in chimney carbon soot [49]. The present results establish distinct types of carbon phases and offer insight into their outstanding structural and electronic properties.

[1] A. T. Balaban, Comput. Math. Appl. **17**, 397 (1989).

[2] E. A. Belenkov and V. A. Greshnyakov, Phys. Solid State **55**, 1754 (2013).

[3] J. T. Wang, C. F. Chen, and Y. Kawazoe, Sci. Rep. **3**, 03077 (2013).

[4] R. Clarke and C. Uher, Adv. Phys. **33**, 469 (1984).

[5] H. Sumiya and T. Irifune, J. Mater. Res. **22**, 2345 (2007).

[6] T. Irifune, A. Kurio, S. Sakamoto, T. Inoue, and H. Sumiya, Nature (London) **421**, 599 (2003).

[7] R. Hoffmann, A. A. Kabanov, A. A. Golov, and D. M. Proserpio, Angew. Chem., Int. Ed. **55**, 10962 (2016).

[8] H. W. Kroto, J. R. Heath, S. C. Obrien, R. F. Curl, and R. E. Smaliey, Nature (London) **318**, 162 (1985).

[9] S. Iijima, Nature (London) **354**, 56 (1991).

[10] K. S. Novoselov, A. K. Geim, S. V. Morozov, D. Jiang, Y. Zhang, S. V. Dubonos, I. V. Grigorieva, and A. A. Firsov, Science **306**, 666 (2004).

[11] M. M. Haley, S. C. Brand, and J. J. Pak, Angew. Chem., Int. Ed. Engl. **36**, 836 (1997).

[12] X. L. Sheng, Q. B. Yan, F. Ye, Q. R. Zheng, and G. Su, Phys. Rev. Lett. **106**, 155703 (2011).

[13] C. J. Pickard and R. J. Needs, Phys. Rev. B **81**, 014106 (2010).

[14] J. Y. Jo and B. G. Kim, Phys. Rev. B **86**, 075151 (2012).

[15] J. T. Wang, C. F. Chen, E. G. Wang, and Y. Kawazoe, Sci. Rep. **4**, 04339 (2014).

[16] H. A. Calderon, I. Estrada-Guel, F. Alvarez-Ramírez, V. G. Hadjiev, and F. C. Robles Hernandez, Carbon **102**, 288 (2016).

[17] J. T. Wang, H. Weng, S. Nie, Z. Fang, Y. Kawazoe, and C. F. Chen, Phys. Rev. Lett. **116**, 195501 (2016).

[18] Y. Cheng, X. Feng, X. T. Cao, B. Wen, Q. Wang, Y. Kawazoe, and P. Jena, Small **13**, 1602894 (2017).

[19] Z. Zhao, Y. Hang, Z. Zhang, and W. Guo, Phys. Rev. B **100**, 115420 (2019).

[20] J. T. Wang, S. Nie, H. Weng, Y. Kawazoe, and C. F. Chen, Phys. Rev. Lett. **120**, 026402 (2018).

[21] P. Németh, L. A. J. Garvie, T. Aoki, N. Dubrovinskaia, L. Dubrovinsky, and P. R. Buseck, Nat. Commun. **5**, 5447 (2014).

[22] C. Y. He, X. Z. Shi, S. J. Clark, J. Li, C. J. Pickard, T. Ouyang, C. X. Zhang, C. Tang, and J. X. Zhong, Phys. Rev. Lett. **121**, 175701 (2018).

[23] W. L. Mao, H. K. Mao, P. J. Eng, T. P. Trainor, M. Newville, C. C. Kao, D. L. Heinz, J. Shu, Y. Meng, and R. J. Hemley, Science **302**, 425 (2003).

[24] Q. Li, Y. M. Ma, A. R. Oganov, H. B. Wang, H. Wang, Y. Xu, T. Cui, H. K. Mao, and G. T. Zou, Phys. Rev. Lett. **102**, 175506 (2009).

[25] K. Umemoto, R. M. Wentzcovitch, S. Saito, and T. Miyake, Phys. Rev. Lett. **104**, 125504 (2010).

[26] J. T. Wang, C. F. Chen, and Y. Kawazoe, Phys. Rev. Lett. **106**, 075501 (2011).

[27] M. Amsler, J. A. Flores-Livas, L. Lehtovaara, F. Balima, S. A. Ghasemi, D. Machon, S. Pailhès, A. Willand, D. Caliste, S. Botti, A. San Miguel, S. Goedecker, and M. A. L. Marques, Phys. Rev. Lett. **108**, 065501 (2012).

[28] Z. S. Zhao, B. Xu, X. F. Zhou, L. M. Wang, B. Wen, J. L. He, Z. Y. Liu, H. T. Wang, and Y. J. Tian, Phys. Rev. Lett. **107**, 215502 (2011).

[29] H. Y. Niu, X. Q. Chen, S. B. Wang, D. Z. Li, W. L. Mao, and Y. Y. Li, Phys. Rev. Lett. **108**, 135501 (2012).

[30] Z. S. Zhao, F. Tian, X. Dong, Q. Li, Q. Q. Wang, H. Wang, X. Zhong, B. Xu, D. L. Yu, J. L. He, H. T. Wang, Y. M. Ma, and Y. J. Tian, J. Am. Chem. Soc. **134**, 12362 (2012).

[31] J. T. Wang, C. F. Chen, and Y. Kawazoe, J. Chem. Phys. **137**, 024502 (2012).

[32] Z. Z. Li and J. T. Wang, Phys. Chem. Chem. Phys. **20**, 22762 (2018).

[33] J. T. Wang, C. F. Chen, and Y. Kawazoe, Phys. Rev. B **85**, 033410 (2012).

[34] J. Dong, Z. Yao, M. Yao, R. Li, K. Hu, L. Zhu, Y. Wang, H. Sun, B. Sundqvist, K. Yang, and B. B. Liu, Phys. Rev. Lett. **124**, 065701 (2020).

[35] R. B. Aust and H. G. Drickamer, Science **140**, 817 (1963).

[36] Z. Z. Li, C. S. Lian, J. Xu, L. F. Xu, J. T. Wang, and C. F. Chen, Phys. Rev. B **91**, 214106 (2015).

[37] K. Yamada, Carbon **41**, 1309 (2003).

[38] M. T. Yin, Phys. Rev. B **30**, 1773 (1984).

[39] R. L. Johnston and R. Hoffmann, J. Am. Chem. Soc. **111**, 810 (1989).

[40] M. D. Knudson, M. P. Desjarlais, and D. H. Dolan, Science **322**, 1822 (2008).

[41] R. Biswas, R. M. Martin, R. J. Needs, and O. H. Nielsen, Phys. Rev. B **30**, 3210 (1984).

[42] H. Vora and T. J. Moravec, J. Appl. Phys. **52**, 6151 (1981).

[43] J. K. Burdett and S. Lee, J. Am. Chem. Soc. **107**, 3063 (1985).

[44] P. Liu, H. Cui, and G. W. Yang, Cryst. Growth Des. **8**, 581 (2008).

[45] J. Zhang, R. Wang, X. Zhu, A. Pan, C. Han, X. Li, Z. Dan, C. Ma, W. Wang, H. Su, and C. Niu, Nat. Commun. **8**, 683 (2017).

[46] J. T. Wang, C. F. Chen, H. Mizuseki, and Y. Kawazoe, Phys. Chem. Chem. Phys. **20**, 7962 (2018).

[47] S. H. Zhang, J. Zhou, Q. Wang, X. S. Chen, Y. Kawazoe, and P. Jena, Proc. Natl. Acad. Sci. USA **112**, 2372 (2015).

[48] Y. Fujii, M. Maruyama, N. T. Cuong, and S. Okada, Phys. Rev. Lett. **125**, 016001 (2020). This article has been retracted; see **125**, 079901(E) (2020).

[49] D. Pantea, S. Brochu, S. Thiboutot, G. Ampleman, and G. Scholz, Chemosphere **65**, 821 (2006).

[50] Z. Z. Li, J. T. Wang, H. Mizuseki, and C. F. Chen, Phys. Rev. B **98**, 094107 (2018).

[51] J. Tersoff, Phys. Rev. B **39**, 5566 (1989).

[52] G. Kresse and J. Furthmüller, Phys. Rev. B **54**, 11169 (1996).

[53] R. Armiento and A. E. Mattsson, Phys. Rev. B **72**, 085108 (2005).

[54] P. E. Blöchl, Phys. Rev. B **50**, 17953 (1994).

[55] A. V. Krukau, O. A. Vydrov, A. F. Izmaylov, and G. E. Scuseria, J. Chem. Phys. **125**, 224106 (2006).

[56] A. Togo, F. Oba, and I. Tanaka, Phys. Rev. B **78**, 134106 (2008).

[57] B. Silvi and A. Savin, Nature (London) **371**, 683 (1994).

[58] See Supplemental Material at http://link.aps.org/supplemental/10.1103/PhysRevB.102.184106 for the original data BC14-ELFCAR. The ELF map can be plotted with the original data. The ELF map in Fig. 1(c) appears to be localized on some C_3 atoms. This illusion stems from the viewing angle.

[59] F. D. Murnaghan, Proc. Natl. Acad. Sci. USA **30**, 244 (1944).

[60] F. Birch, Phys. Rev. **71**, 809 (1947).

[61] A. F. Goncharov, J. C. Crowhurst, J. K. Dewhurst, S. Sharma, C. Sanloup, E. Gregoryanz, N. Guignot, and M. Mezouar, Phys. Rev. B **75**, 224114 (2007).

[62] F. Occelli, P. Loubeyre, and R. Letoullec, Nat. Mater. **2**, 151 (2003).

[63] X-Q. Chen, H. Niu, D. Li, and Y. Li, Intermetallics **19**, 1275 (2011).

[64] Z. J. Wu, E. J. Zhao, H. P. Xiang, X. F. Hao, X. J. Liu, and J. Meng, Phys. Rev. B **76**, 054115 (2007).

[65] V. V. Brazhkin, M. V. Kondrin, A. G. Kvashnin, E. Mazhnik, and A. R. Oganov, arXiv:2007.08912.

[66] S. Saha, W. von der Linden, and L. Boeri, arXiv:2007.09254.

[67] X. Q. Chen, H. Niu, C. Franchini, D. Li, and Y. Li, Phys. Rev. B **84**, 121405(R) (2011).

[68] D. Selli, I. A. Baburin, R. Martonak, and S. Leoni, Phys. Rev. B **84**, 161411(R) (2011).

[69] J. T. Wang, C. F. Chen, D. S. Wang, H. Mizuseki, and Y. Kawazoe, J. Appl. Phys. **107**, 063507 (2010).

[70] The strong peak at $30°$ was also attributed to all-sp^2 graphene network structures such as the bco-C_{16} [17], bct-C_{16} [18], and ors-C_{16} carbon phases [19].

[71] R. Hoffmann, A. A. Kabanov, A. A. Golov, and D. M. Proserpio, Samara Carbon Allotrope Database, http://sacada.sctms.ru.

[72] P. Avery, X. Wang, C. Oses, E. Gossett, D. M. Proserpio, C. Toher, S. Curtarolo, and E. Zurek, npj Comput. Mater. **5**, 89 (2019).

[73] J. T. Wang, C. F. Chen, and Y. Kawazoe, Phys. Rev. B **84**, 012102 (2011).

[74] J. T. Wang, C. F. Chen, H. Mizuseki, and Y. Kawazoe, Phys. Rev. Lett. **110**, 165503 (2013).